Mesoporous Materials

Nano-Designed Enzyme–Functionalized Hierarchical Metal–Oxide Mesoporous Thin Films: En Route to Versatile Biofuel Cells

Martín G. Bellino and Galo J. A. A. Soler-Illia*

Mesoporous oxide thin films (MOTF) are amenable to be integrated to most electronic devices, displaying properties derived from pore architecture that combine the accessibility of the mesopore system, the protective properties of the matrix and surface functionalization.[1,2] It has been demonstrated that MOTF represent an excellent host for a variety of active enzymes[3,4] and metal nanoparticles.[5–7] Particularly, silver nanoparticle patterns, can be produced within titania MOTF by UV-lithography, permitting to produce highly controlled, robust and conductive metal-oxide nanocomposites.[8,9] A desired evolution in MOTF is the possibility for fabricating versatile scaffolds for applications in bioelectronic devices. In this work, we show that this ambitious evolution can be realized by exploiting the advantages of tuning the nanoarchitecture and the conductivity in mesoporous nanocomposite thin films functionalized with electroactive enzymes, leading to easy to prepare versatile biofuel cells with unprecedented high power.

A typical biofuel cell (BFC) reactor consists of an anode and a cathode compartment that are separated by an ion-selective membrane.[10,11] In the case of glucose-oxygen based BFCs, glucose is oxidized at the anode, generally via glucose oxidase (GOx), and dioxygen is reduced at the cathode generally by laccase. The controlled localization and efficient "wiring" of these enzymes onto the active electrode is central in BFC construction giving rise to single compartment BFCs.[10,11] The vast majority of enzymatic fuel cells employ shuttle species such as redox-active compounds as mediators to establish an electron transfer between enzymes and a variety of nanostructured electrodes, such as carbon nanotube supports,[12] and nanoparticulate gold substrates.[13] An important issue for the scale-up production of versatile BFCs is their ability to be processed as thin films compatible with the electronics industry, leading to an easy miniaturization and integration with microfluidic and microelectronic systems. The development and application of thin film electrodes for high power BFC in the absence of mediators are eagerly awaited, but weak power of only a few μW cm^{-2} values has been reported to date.[11,14–18]

As proof of concept, this Communication reports that a modular combination of building blocks of different nature, such as hierarchical mesoporous titania thin films, Ag nanoparticles and electroactive enzymes (GOx and laccase) leads to a very efficient ultrathin biofuel cell system without the need to add mediators, which stands above the state-of-the art performance. This methodology is fully compatible with the techniques and substrates used in the sensor, microfluidic and microelectronics industry, opening the path to portable electronic and self-powered implantable devices. An additional advantage is the possibility to add electroactive enzymes with electron accepting or withdrawing capacity, without modifying the processes involved in the preparation of the electrode scaffolds.

Bioanodes and biocathodes were prepared on glass substrates in three stages as schematised in **Figure 1**. A 100 nm thick layer of sol-gel silica was first deposited as a buffer layer on glass, in order to favour titania crystallization.[19] Mesoporous titania thin films were produced by dip–coating the modified glass substrates in water/alcohol acidic solutions containing an inorganic precursor ($TiCl_4$) and a pore template (Pluronics F127).[20] A co-template (poly (propylene glycol), PPG) was added in order to attain hierarchical porous structure.[21] After deposition, films were stabilized and calcined at 350 °C for 2 hours. Depending on the initial sol composition, transparent and crack-free thin films exhibit uniform 9 nm pore size (conventional templated films, 78 nm thick, hereafter, C9 samples; See Figure S1 in the Supporting Information) or hierarchical pore size distributions with a dual pore size distribution centered in 13 and 38 nm diameter, in the presence of PPG (90 nm thick, hereafter, H13–38 samples; See **Figure 2**a,c and Figure S1 in the Supporting Information). It is worth mentioning that ~6 nm inter-mesopore neck size distributions are attained in the C9 uniform architecture and between the smaller mesopore population in the hierarchical H13–38 thin films. The larger pores in the H13–38 film are evenly distributed along the whole film thickness and interconnected through much wider necks.[21] In a second step, Ag nanoparticles (NP) were deposited through impregnation-photodeposition, as previously reported.[8,9] Silver

Dr. M. G. Bellino, Prof. G. J. A. A. Soler-Illia
Gerencia Química, Comisión Nacional
de Energía Atómica
Av. Gral. Paz 1499, San Martín
B1650KNA, Argentina
E-mail: mbellino@cnea.gov.ar

DOI: 10.1002/smll.201302616

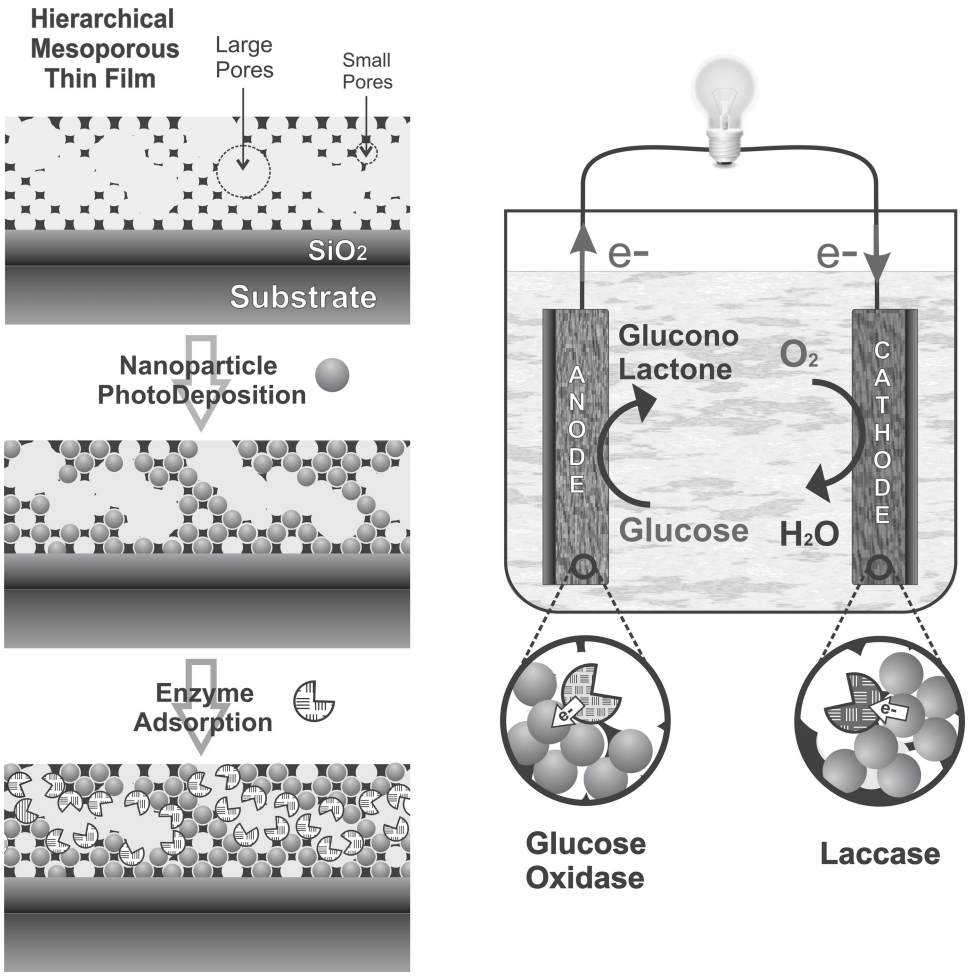

Figure 1. Right: Sketch representation of key steps of the enzyme-functionalized nanocomposite thin film electrode fabrication. Left: Schematic illustration of single compartment GBFC. At the anode, glucose is oxidized to gluconolactone, where the electrons are transferred from the GOx to electrode. At the cathode, electrons are transferred from electrode to laccase where dioxygen is reduced to water.

nanoparticle formation was evident by the development of a dark brownish color evenly distributed throughout the film due to surface plasmon resonance of Ag NPs formed within the titania films (Figure S2). Homogeneous metal deposition leads to NP diameter of ca. 10 nm, a size similar to the one reported in conventional mesoporous films.[8,9] Interestingly, in the hierarchical films, the silver nanoparticle diameter coincides with the smaller pores, and no NP deposition was observed within the large pore population (Figure 2d). This might be due to a more efficient Ag^+ preconcentration in the smaller mesopores that leads to faster silver reduction in the most confined spaces. The pore volume filling was estimated from the Ag:Ti ratio by Energy Dispersive Spectroscopy (EDS),[8,9] resulting in an occupied pore volume of near 60% in both kinds of titania films. In a third step, film biofunctionalization was performed by immersing the previously prepared nanocomposite films in aqueous GOx and Laccase solutions (1 mg/mL) for 60 min under agitation at room temperature, for the preparation of bioanodes and biocathodes respectively.

A membrane-less glucose/O_2 biofuel cell (sketched in Figure 1) was then elaborated by associating both enzyme-functionalized electrodes immersed 4 mm apart in a one-compartment cell containing phosphate buffer solutions (pH 7) with 0.05 mol L^{-1} glucose operating at 20 °C. The recorded open-circuit potential (OCP) was 0.91 ± 0.05 V in the H13–38 thin films based GBFC (See Figure S3 in the Supporting Information), corresponding to the ideal difference between the redox potentials of the two biocatalysts.[22] In contrast, a much lower OCP (~0.4 V) was observed in the C9 electrodes. The OCP values obtained in the hierarchical nanocomposite GBFC already reflect a more efficient electrical connection of enzymes when compared to the C9-based GBFC, indicating that highly active immobilized enzymes are available in the H13–38 based nanostructure.

Power density as a function of current density of the resulting GBFC is shown in **Figure 3**. The activity of the C9 nanocomposite films exposed to enzyme solutions was 15 μW/cm^2. The hierarchical nanocomposites present a peak power density of 403 μW/cm^2 at a voltage of 0.68 V, which is an outstanding value for the construction of separator-less, mediator-free high performance glucose/O_2 biofuel cell. The operational voltage obtained in our GBFC suffices to supply electronic devices and implanted biomedical devices that usually require at least an operating voltage of 0.5–0.6 V.[23] The strong differences in bioactivity between both film types can be attributed to the substantially different incorporation

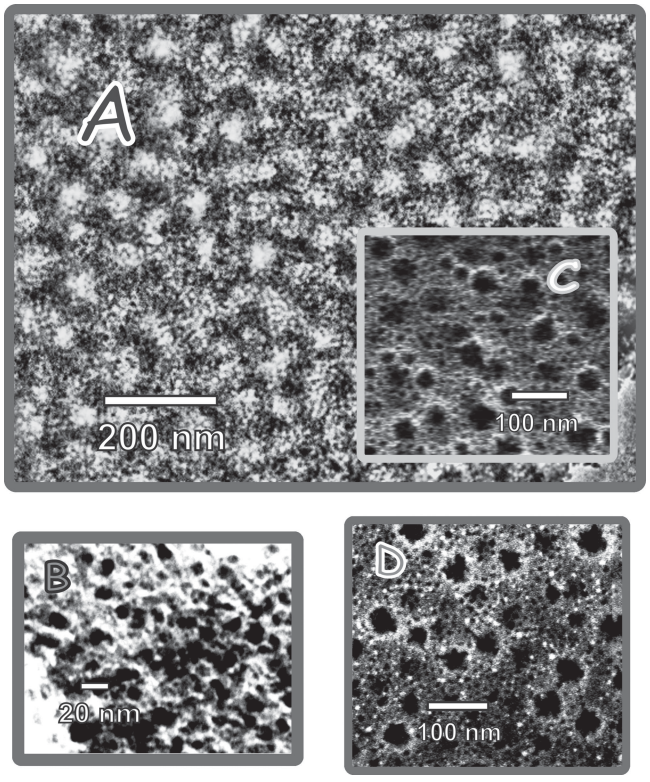

Figure 2. Nanoarchitecture of hierarchically porous nanocomposite scaffolds used in this study: TEM imagine of hierarchical mesoporous film showing bimodal porosity (a), and the presence of nanoparticles between 8–10 nm in diameters into the smaller pores after Ag photodeposition (b). FE-SEM imagines of hierarchical mesoporous film before (c) and after (d) infiltration with Ag NPs. Note that silver nanoparticles was selectively located in smaller size mesopores.

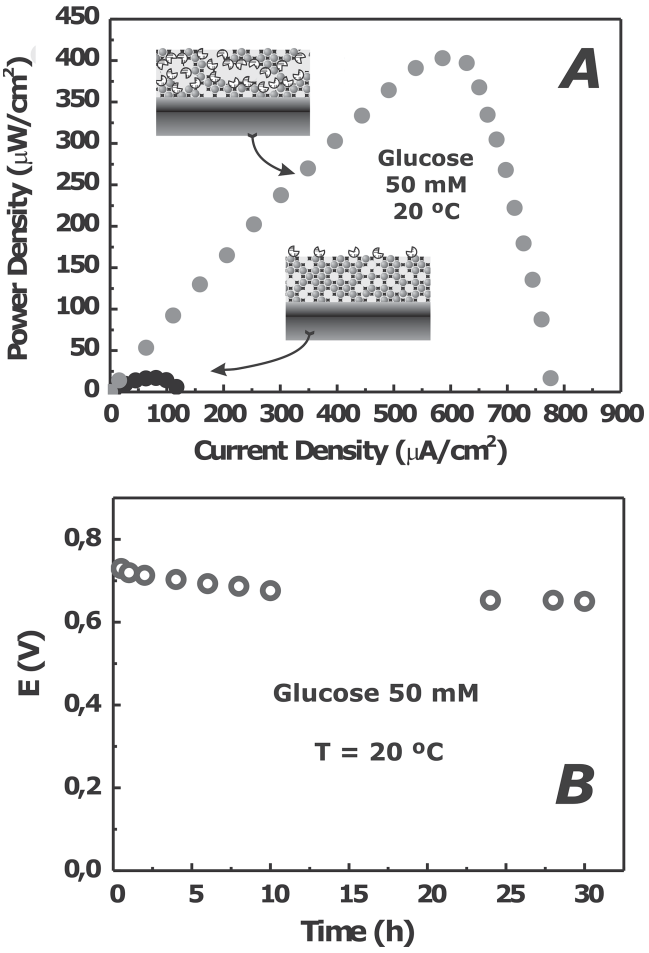

Figure 3. (a) Dependence of power density on current density for a biofuel cell made with conventional (black circle) and hierarchical (red circle) mesoporous titania/silver nanoparticle nanocomposite scaffolds in a quiescent phosphate buffered 50 mM glucose solution under air at 20 °C. (b) Long-term performance of voltage on time for continuous discharge under 500 μA cm^{-2} in 0.05 mol L^{-1} glucose solution.

of GOx and laccase within their pore systems. UV-visible spectra of enzyme-containing solutions before and after pre-incubation (See Supporting Information Figure S4) indicate that enzymes are efficiently incorporated into the hierarchical H13–38 films. However, only a very small amount of enzyme is adsorbed by the mesoporous C9 films, leading to an electrode performance comparable with mediator-less cells reported in the literature.[11] The high enzyme adsorption in the hierarchical electrodes can be explained in terms of the large interpore neck size attained into the large porosity of the H13–38 sample that permits the access of large macromolecules. These H13–38 nanocomposite scaffolds permit to achieve a high immobilization degree (ca. 7 and 11 μg/cm^2 for GOx and Laccase respectively, See the Supporting Information) when compared to traditional architecture where the protein sequestration is negligible. This effect has been previously observed in the adsorption of DNA polymerases in the whole pore volume of hierarchically structured MTTF.[3] Laccase and GOx present sizes in the same order of magnitude, of diameters of ca. 5.9 and 6.7 nm respectively;[24] in addition, the active GOx species is composed of higher weight dimers. Even when pore sizes in the C9 mesoporous films are large enough, the smaller interpore necks of C9 are comparable or slightly smaller than the enzyme diameter, thus preventing its incorporation in significant quantities. The larger pores in H13–38 act as cages for the redox enzymes, interconnected by smaller pores that allow for the supply of reactants. The silver NP also have a key role in this bionanocomposite, probably improving the contact between the enzyme and the electrode, as reported in sensors.[25] In our case, in addition to the improved electron transfer properties, the Ag° pore filling achieved in the conditions reported here (i.e., ca. 60% pore volume filling) corresponds to an electrically percolated NP network.[9] These two factors contribute to the optimum electrical performance of the electrodes. Control experiments performed in NP-laden films in the absence of enzyme or in the biofunctionalized titania electrodes in absence of silver nanoparticles showed no activity, reinforcing the hypothesis that all three components of the system (i.e., matrix, NP and enzymes) are necessary to produce an efficient BFC. The titania matrix could also play a fundamental role in enzyme wiring and electron transfer at the oxide–metal interface.[26]

The appearance of strong currents that correspond to the catalytic response of immobilized enzymes in the biofuntionalized H13–38 electrodes (See chronoamperometric and polarization curves of bioelectrodes in Supporting Information Figure S5) confirms the excellent activity of these

NANO MICRO small

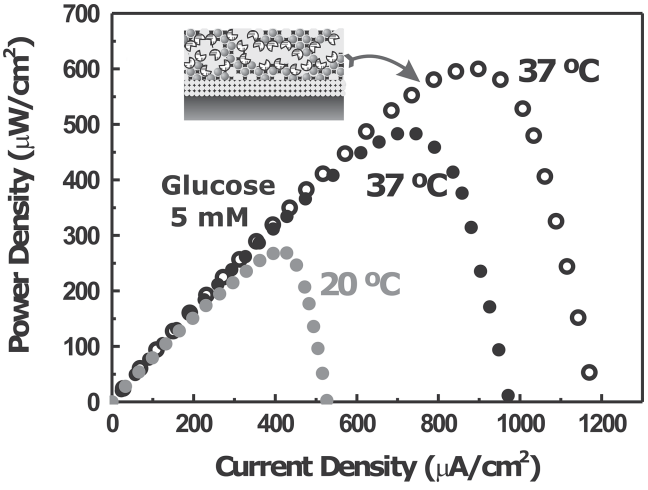

Figure 4. Power density as function of current density obtained from hierarchical mesoporous titania/silver nanoparticle nanocomposite scaffolds based biofuel cell in a quiescent air-saturated phosphate buffered saline solution of 5 mM glucose concentration. The open circles show the improve biofuel cell performance due to the presence of a mesoporous silica membrane at the bottom in a nanoengineered bilayer structure.

novel bioelectrodes that allows for advanced biofuel cell performances. The apparent activity estimated from the current density values recorded for both electrodes (128 and 13 U mg^{-1}, for the bioanode and biocathode, respectively, see details in Supporting Information) resulted close to the activity of free enzymes in solution.

In addition to high power density, good fuel-cell stability is essential for practical applications. Degradation can occur either by a reduction in enzyme stability under operation, but the lifetime may be increased by immobilization. To test the stability of the BFC, we studied the evolution of the cell operated under a constant current density of 500 μA cm^{-2}, near the maximum achieved power density. Only about 10% loss in voltage output was observed after continuous operation for 30 h, as shown in Figure 3b. The power density dependence on the cell voltage was recorded after 10 days storage of GBFC in the buffer solution at room temperature leading to only a 8% decrease for the maximum power density (Figure S6A). In addition, OCP and current density of the bioelectrodes immersed in buffer solution were periodically measured (See SI Figure S6 B,C), showing that after a slight initial decrease during the first 2 days, these parameters remained stable in both bioelectrodes. The catalytic currents maintained more than 85% of its initial value after storage for 10 days, indicating a good lifetime for the bioelectrodes.

In order to be able to integrate GBFC for potential applications in self-powered implantable devices, we tested the power density of our GBFC in physiological conditions. **Figure 4** shows the performances of the GBFC in phosphate buffer (pH = 7.2) containing 5×10^{-3} mol L^{-1} glucose and 0.14 M NaCl, corresponding to the concentrations in extracellular body fluids.[10] Even at low glucose concentration and the possible inhibition of laccase by chloride ions,[27] the GBFC exhibited excellent performance (maximum power density = 273 μW/cm^2 at 0.64 V and 487 μW/cm^2 at 0.66 V, when the GBFC were evaluated at 20 °C and 37 °C, respectively). The resistance of wired laccase towards chloride inhibition must be attributed to the improved performance of immobilized enzymes.[4]

The power densities per geometrical area obtained of the resulting GBFC at the different conditions tested was two orders of magnitude higher than those mediator-less film type biofuel cells yielded,[11,14–18] and even superior than most reported in the literature via redox mediators.[11,13,28–34] The specific power of our ultrathin GBFC (per unit of volume of electrode) exceeds by four orders of magnitude the power density obtained for the best performance reported for a GBFC that was based on compressed carbon nanotube disks of 3 mm thick (reached 1 mW/cm^{-2} under physiological conditions).[23] This result suggests that the hierarchical nanocomposite matrix here reported allows for an improved connection of large number of enzymes.

In order to improve the transport properties of the systems, an intermediate SiO_2 mesoporous silica layer with 3 nm diameter pores (see SI Figure S1) was inserted between the glass substrate and the titania films.[35] No Ag deposition takes place inside the silica mesoporous films,[8] and enzymes do not enter the 3 nm diameter mesopores in the SiO_2 layer. A significant improvement in power density was observed for this nanoengineered multilayer. From Figure 4, it is clear that the addition of a mesoporous silica underlayer leads to deliver a maximum power density of 602 μWcm^{-2} at 0.68 V. The mesoporous silica film facilitates mass transport of products and reactants to/from electrodes. This interesting result obtained in the nanoengineered bilayer shows a promising direction to enhance the performance of thin film BFCs.

In summary, in this work we have demonstrated for the first time that high power and stable membrane-less, mediator-free glucose BFC can be achieved using a flexible concept: enzyme-functionalized hierarchically porous metal–oxide nanocomposite thin film electrodes. These bio-nanocomposites have multiple tunable functions arising from their nanocomponents, i.e., the enzymes (biocatalysis), the matrix (efficient permeation of the species) and the nanoparticles (enzyme wiring, electrical conductivity). In contrast to the classical fabrication of electrodes on conductive substrates, this straightforward method leads to robust bioelectrodes directly on microscope glass slides. The power densities here obtained represent an increase of two orders of magnitude with respect to previously reported GBFC, including operation in physiological conditions. The synergy between excellent performance, mediator-less operation, thin film architecture, simplicity and low cost of the bioelectrodes presented here open a new scenario in mesoporous material applications in portable electronics or implantable biomedical devices, which require and process signals on a low-energy basis (nW to μW).[36] Finally, it is worth remarking the simplicity and flexibility of the advanced methodology presented here that permits to be extended to a variety of redox enzymes for applications in biosensors, signal transducing, or light harvesting.

Experimental Section

Synthesis and Deposition of Mesoporous Layers: Standard microscope glass slides (76 mm long, 26 mm wide, 1.1 mm thick) were washed thoroughly with dextran, and rinsed successively with water, ethanol, and acetone. An intermediate layer of non-mesoporous or mesoporous SiO_2 is first deposited by dip coating. $Si(OEt)_4$ (TEOS) was used as the inorganic precursor and cethyltrimethylammonium bromide (CTAB, Alfa Aesar) was selected as the template. TEOS was prehydrolyzed by refluxing for 1 h in a water/ethanol solution; $[H_2O]/[Si. = 1$; $[EtOH]/[TEOS. = 5$. To this prehydrolyzed solution was added surfactant, alcohol, and acidic water in order to prepare the precursor solutions, with final composition TEOS:EtOH:H_2O (0.1 M HCl):CTAB equal to 1:40:5:0.1 mol ratios. Non-mesoporous films were made as described, but in the absence of the template. The films were then subjected to a consolidation thermal treatment, which consisted of heating at 60 °C for 24 h and at 130 °C for another 24 h and finally at 200 °C during 2 h. Next, the mesoporous layer were incorporated in second stages. Solutions for conventional mesoporous titania thin films were prepared by adding an organic template $(EO)_{106}(PO)_{70}(EO)_{106}$ (commercial name F127, Aldrich Inc.) to a $TiCl_4$:EtOH solution. The final composition of the precursos solution was $TiCl_4$:EtOH:H_2O:F127 = 1:40:10:0.0075. Hierarchical mesoporous thin films were synthesized by adding a low-cost swelling agent (PPG = polypropylene glycol 4000 – Alfa Aesar GMBH&Co). Molar ratios in the precursor sols were $TiCl_4$:BuOH:H_2O:F127:PPG = $1:40:10:4 \times 10^{-3}:6.2 \times 10^{-3}$. To coat the glass substrates we used a dip-coating process at a withdrawal rate of 0.5 mm s^{-1} and a relative humidity (RH) of 20%. After the deposition, the samples were introduced into a 50% relative humidity chamber for 24 hours, then thermally stabilized at 60 °C and 130 °C during 24 h. To stabilize the overall structure and to remove the organic template we made a thermal treatment at 350 °C for 1 h (ramp 1 °C/min).

Photodeposition of Silver NPs: The films were immersed in a 1 M $AgNO_3$ water-ethanol solution (1:1 volume ratio) for 10 min under agitation in the dark to optimize metal infiltration. Subsequently, films were placed in a shallow plastic container. A few milliliters of the Ag^+ solution described above was added until the film was completely immersed. Finally, the container was placed 1 cm below a UV tube lamp (Phillips, 15 W, emission peak at 355 nm) for 90 min. After deposition, the sample was withdrawn from the bath and thoroughly rinsed with water and ethanol.

Enzyme Immobilization: Glucose oxidase (GOx) from Aspergillus niger (181 U mg^{-1} solid) and laccase from Trametes versicolor (14 U mg^{-1} solid) were purchased from Sigma-Aldrich and used without further purification. Protein immobilization was achieved by immersing the so-prepared porous films in a 1 mg/mL enzyme aqueous solution for 60 min under agitation at room temperature. The films were then thoroughly rinsed with water and stored in a clean box at ambient conditions. The concentrations of protein in the solution before and after enzyme adsorption were determined by UV-vis spectroscopy at 280 nm.

Instrumentation: The electrochemical characterization and the biofuel cell tests were performed with a TEQ-03 Potentiostat/Galvanostat. All electrochemical experiments were carried out in a conventional three-electrode cell except for the biofuel cell experiments. A Pt wire was used as the counter electrode and the reference was a SCE. Glucose solutions were prepared in phosphate buffer 0.2 M (pH 7) at least 24 h before its use. All runs were carried out in triplicate at a constant temperature, using a water bath. Field emission-scanning electron microscopy (FE-SEM) images were taken with a Zeiss Leo 982 Gemini electron microscope using the secondary-electron mode and an in-lens detector to improve resolution. Transmission electron microscopy (TEM) images were obtained using a Phillips CM 200 electron microscope. UV-vis spectroscopy was performed employing a Hewlett-Packard 8453 spectrophotometer in transmission mode. Film thickness, volume and pore size distribution values were obtained from environmental ellipsometric porosimetry (EEP, SOPRA GES5A). Pore diameters were obtained from the pore size distribution function using a simple Kelvin model with a precision of ±0.5 nm.

Supporting Information

Supporting Information is available from the Wiley Online Library or from the author.

Acknowledgements

The authors acknowledge valuable discussions with E. D. Martinez and P. Scodeller. This work was supported by CONICET (PIP 00186) and ANPCyT (PICT 1848 and 2087) and PICT 2969. M.G.B. and G. J. A. A. S-I are members of CONICET.

[1] C. Sanchez, C. Boissière, D. Grosso, C. Laberty, L. Nicole, *Chem. Mater.* **2008**, *20*, 682–737.
[2] G. J. A. A. Soler-Illia, P. C. Angelomé, M. C. Fuertes, A. Calvo, A. Wolosiuk, A. Zelcer, M. G. Bellino, E. D. Martínez, *J. Sol-Gel Sci. Technol.* **2011**, *57*, 299–312.
[3] M.G. Bellino, I. Tropper, H. Duran, A. E. Regazzoni, G. J. A. A. Soler-Illia, *Small* **2010**, *6*, 1221–1225.
[4] M. G. Bellino, A. E. Regazzoni, G. J. A. A. Soler-Illia, *ACS Appl. Mater. Interfaces* **2010**, *2*, 360–365.
[5] M. Andersson, H. Birkedal, N. R. Franklin, T. Ostomel, S. Boettcher, A. E. C. Palmqvist, G. D. Stucky, *Chem. Mater.* **2005**, *17*, 1409–1415.
[6] M. D. Perez, E. Otal, S. A. Bilmes, G. J. A. A. Soler-Illia, E. L. Crepaldi, D. Grosso, C. Sanchez, *Langmuir* **2004**, *20*, 6879–6886.
[7] Y. Plyuto, J. M. Berquier, C. Jacquiod, C. Ricolleau, *Chem. Commun.* **1999**, *17*, 1653–1654.
[8] E. D. Martínez, M. G. Bellino, G. J. A. A. Soler-Illia, *ACS Appl. Mater. Interfaces* **2009**, *1*, 746–749.
[9] E. D. Martínez, L. Granja, M. G. Bellino, G. J. A. A. Soler-Illia, *Phys. Chem. Chem. Phys.* **2010**, *12*, 14445–14448.
[10] S. C. Barton, J. Gallaway, P. Atanassov, *Chem. Rev.* **2004**, *104*, 4867–4886.
[11] M. H. Osman, A. A. Shah, F. C. Walsh, *Biosens. Bioelectron.* **2011**, *29*, 3087–3102.
[12] F. Gao, L. Viry, M. Maugey, P. Poulin, N. Mano, *Nat. Commun.* **2010**, *1*, 2.
[13] O. Yehezkeli, R. Tel-Vered, S. Raichlin, I. Willner, *ACS Nano* **2011**, *5*, 2385–2391.
[14] M. Falk, Z. Blum, S. Shleev, *Electrochim. Acta* **2012**, *82*, 191–202.

[15] V. Coman, C. Vaz-Domínguez, R. Ludwig, W. Harreither, D. Haltrich, A. L. De Lacey, T. Ruzgas, L. Gorton, S. Shleev, *Phys. Chem. Chem. Phys.* **2008**, *10*, 6093–6096.
[16] X. Wang, M. Falk, R. Ortiz, H. Matsumura, J. Bobacka, R. Ludwig, M. Bergelina, L. Gorton, S. Shleev, *Biosens. Bioelectron.* **2012**, *31*, 219–225.
[17] V. Coman, R. Ludwig, W. Harreither, D. Haltrich, L. Gorton, T. Ruzgas, S. A. Shleev, *Fuel cells* **2010**, *10*, 9–16.
[18] S. C. Wang, F. Yang, M. Silva, A. Zarow, Y. Wang, Z. Iqbal, *Electrochem. Commun.* **2009**, *11*, 34–37.
[19] U. L. Štangar, U. Černigoj, P. Trebše, K. Maver, S. Gross, *Monatsh. Chem.* **2006**, *137*, 647–655.
[20] E. L. Crepaldi, G. J. A. A. Soler-Illia, D. Grosso, F. Cagnol, F. Ribot, C. Sanchez, *J. Am. Chem. Soc.* **2003**, *125*, 9770–9787.
[21] L. Malfatti, M. G. Bellino, P. Innocenzi, G. J. A. A. Soler-Illia, *Chem. Mater.* **2009**, *21*, 2763–2769.
[22] A. Zebda, L. Renaud, M. Cretin, F. Pichot, C. Innocent, R. Ferrigno, S. Tingry, *Electrochem. Commun.* **2009**, *11*, 592–595.
[23] A. Zebda, C. Gondran, A. Le Goff, M. Holzinger, P. Cinquin, S. Cosnier, *Nat. Commun.* **2011**, *2*:370doi: 10.1038/ncomms1365.
[24] estimated from the PDB files, available in http://www.rcsb.org/pdb/explore.do?structureId=1KYA and http://www.rcsb.org/pdb/explore/jmol.do?structureId=1CF3&bionumber=1.
[25] X. Rena, X. Menga, D. Chena, F. Tanga, J. Jiao, *Biosens. Bioelectron.* **2005**, *21*, 433–437.
[26] S. J. Bao, C. M. Li, J. F. Zang, X. Q. Cui, Y. Qiao, J. Guo, *Adv. Funct. Mater.* **2008**, *18*, 591–599.
[27] F. Xu, *Biochemistry* **1996**, *35*, 7608–7614.
[28] Y. Tan, W. Deng, Y. Li, Z. Huang, Y. Meng, Q. Xie, M. Ma, S. Yao, *J. Phys. Chem. B* **2010**, *114*, 5016–5024.
[29] H. La Rotta, C. E. Ciniciato, E. R. González, *Enzyme Microbial Technol.* **2011**, *4*, 487–497.
[30] C. Tanne, G. Göbel, F. Lisdat, *Biosens. Bioelectron.* **2010**, *26*, 530–535.
[31] H.-B. Noha, M.-S. Wonb, J. Hwanga, N.-H. Kwona, S. C. Shinc, Y.-B. Shima, *Biosens. Bioelectron.* **2010**, *25*, 1735–1741.
[32] M. Smolander, H. Boer, M. Valkiainen, R. Roozeman, M. Bergelin, J.-E. Eriksson, X.-C. Zhang, A. Koivula, L. Viikari, *Enzyme Microbial Technol.* **2008**, *43*, 93–102.
[33] N. Mano, F. Mao, A. Heller, *J. Am. Chem. Soc.* **2002**, *124*, 12962–12963.
[34] T. Chen, S. C. Barton, G. Binyamin, Z. Gao, Y. Zhang, H.-H. Kim, A. Heller, *J. Am. Chem. Soc.* **2001**, *123*, 8630–8631.
[35] P. C. Angelomé, M. C. Fuertes, G. J. A. A. Soler-Illia, *Adv. Mater.* **2006**, *18*, 397.
[36] Y. Li, F. Qian, J. Xiang, C. M. Lieber, *Mater. Today* **2006**, *9*, 18–27.

Received: August 9, 2013
Revised: February 28, 2014
Published online: March 18, 2014